Curved concrete crownwalls on vertical breakwaters under impulsive wave load

Finite Element Analysis

Gísladóttir, Lára M.; Castellino, Myrta; Dermentzoglou, Dimitrios; Hendriks, Max A.N.; de Girolamo, Paolo; van Gent, Marcel R.A.; Antonini, Alessandro

DOI
10.1016/j.coastaleng.2025.104791

Publication date
2025

Document Version
Final published version

Published in
Coastal Engineering

Citation (APA)
Gísladóttir, L. M., Castellino, M., Dermentzoglou, D., Hendriks, M. A. N., de Girolamo, P., van Gent, M. R. A., & Antonini, A. (2025). Curved concrete crownwalls on vertical breakwaters under impulsive wave load: Finite Element Analysis. *Coastal Engineering*, *201*, Article 104791. https://doi.org/10.1016/j.coastaleng.2025.104791

Coastal Engineering 201 (2025) 104791

Contents lists available at ScienceDirect

Coastal Engineering

journal homepage: www.elsevier.com/locate/coastaleng

Curved concrete crownwalls on vertical breakwaters under impulsive wave load: Finite Element Analysis ☆

Lára M. Gísladóttir [a], Myrta Castellino [b], Dimitrios Dermentzoglou [a], Max A.N. Hendriks [c], Paolo de Girolamo [b], Marcel R.A. van Gent [a,d], Alessandro Antonini [a,*]

[a] Delft University of Technology, Department of Hydraulic Engineering, Stevinweg 1, Delft, 2628CN, The Netherlands
[b] "Sapienza" University of Rome, DICEA, Rome, Italy
[c] Delft University of Technology, Department of Engineering Structures, Stevinweg 1, Delft, 2628CN, The Netherlands
[d] Deltares, Department Coastal Structures and Waves, Boussinesqweg 1, Delft, 2629HV, The Netherlands

ARTICLE INFO

Keywords:
Concrete crownwall
Confined-Crest Impact
FEA structural analysis
Structural dynamic response
Wave–structure interaction

ABSTRACT

Curved concrete crownwalls are commonly installed on vertical breakwaters in deep water to mitigate wave overtopping. This study compares the hydraulic and structural performance of fully curved and recurved crownwalls under impulsive wave loads induced by non-breaking waves, known as Confined-Crest Impact. Using one-way coupled numerical simulations in OpenFOAM and structural analyses in DIANA FEA, we assess the pressure fields and structural responses of the two geometries. Results reveal that while the fully curved crownwall significantly reduces overtopping, it experiences wave forces up to 2.5 times greater than the recurved crownwall, along with longer pressure impulse durations, leading to amplified tensile stresses and higher risk of cracking. In contrast, the recurved crownwall, despite localized peak pressures, benefits from a broader cross-section and linear stress distribution, resulting in better structural performance. These findings underscore the importance of integrating dynamic structural analysis in crownwall design to balance hydraulic efficiency with structural resilience.

1. Introduction

Breakwaters are crucial for securing navigation and berthing within ports and harbors and generally fall into two categories: rubble mound and composite vertical breakwaters (Takahashi, 2002). Composite vertical breakwaters are favored in deep-water regions like the Mediterranean, Japan, and Spain De Girolamo et al. (2019). Crownwalls, often used atop these breakwaters, are used to reduce overtopping discharges without increasing the caisson height (Pedersen and Burcharth, 1992; EurOtop, 2018). To further mitigate overtopping, crownwalls may include features such as overhangs, bullnoses, or fully curved faces aimed to deflect the wave induced water jet along the main structure (EurOtop, 2018; Castellino et al., 2018b; Antonini et al., 2023; Castellino, 2024). When the breakwater's top is shaped as a recurve, it reduces overtopping without increasing height, it also increases wave loading compared to a vertical wall, in some cases leading to impulsive loads that pose risks for the structural integrity (Kortenhaus et al., 2004; Kisacik et al., 2012; Castellino et al., 2018b; Chen et al., 2019).

This study focuses on crownwalls on vertical breakwater exposed to non-breaking waves. Failures, such as the structural collapses observed in Civitavecchia Harbour (Italy) (see Fig. 1a) (Castellino et al., 2018b), Pico Island (Azores, Spain) (Martinelli et al., 2018), and Strand (South Africa) (Schoonees, 2014), as well as cases of sliding and overturning reported on Albrán Island (Spain) (Valdecantos et al., 2014; Negro et al., 2018), underscore the risks associated with recurved designs under impulsive wave loading. Despite these incidents, no standardized design guidelines exist specifically for recurved crownwalls. Consequently, there is a growing need to understand not only the hydraulic loadings but also the structural response of curved crownwalls under impulsive loads to enhance design approaches.

Bagnold (1939) first noted that breaking waves on vertical seawalls can create impulsive pressures, with findings later expanded upon by Cooker and Peregrine (1995), who developed a *pressure-impulse theory*. Further research on impulsive wave forces and the dynamic responses of upright breakwaters were conducted by Oumeraci

☆ Given his role as Editor-in-chief, Marcel R.A. van Gent had no involvement in the peer review of this article and has no access to information regarding its peer-review. Full responsibility for the editorial process for this article was delegated to another journal editor.

* Corresponding author.
E-mail address: a.antonini@tudelft.nl (A. Antonini).

https://doi.org/10.1016/j.coastaleng.2025.104791
Received 16 May 2025; Accepted 20 May 2025
Available online 7 June 2025

Nomenclature

$a_{H,V,SW}$:	Bending moment arms [m]
A:	Cross-sectional area [m^2/m]
b:	Width of cross-sections [m]
B_r:	Overhang length [m]
d:	Water depth [m]
E:	Young's modulus [GPa]
f_{cm}:	Compressive strength of concrete [MPa]
f_{ctm}:	Tensile strength of concrete [MPa]
f_n:	Eigenfrequency [Hz]
F_H:	Horizontal wave force [kN/m]
F:	Total wave force [kN/m]
F_V:	Vertical wave force [kN/m]
H:	Wave height [m]
I_P:	Pressure impulse [kPa s]
I_F:	Force impulse [kN s/m]
I_{zz}:	Second moment of area [m^4]
L_0:	Deep water wavelength [m]
M:	Bending moment [m^4]
P:	Wave pressure [kPa]
P_{Im}:	Impulsive pressure [kPa]
P_{qs+}:	Maximum quasi-static pressure [kPa]
R_c:	Freeboard [m]
r:	Radius of curved crownwalls [m]
SW:	Selfweight of top part of crownwalls [kN/m]
s:	Wave steepness [%]
T:	Wave period [s]
T_n:	Natural period of the structure [s]
T_d:	Impulse duration [s]
u_{xy}:	Total displacement [m]
α:	Rayleigh mass-proportional damping coefficient [1/s]
β:	Rayleigh stiffness-proportional damping coefficient [s]
η:	Free water surface elevation [m]
ν:	Poisson's ratio [−]
ρ:	Density [kg/m^4]
σ_c:	Compressive stresses [MPa]
σ_t:	Tensile stresses [MPa]

et al. (1992), Oumeraci and Kortenhaus (1994), Goda (1994), Shimosako et al. (1995), Takahashi et al. (1999), and more recently by Cuomo et al. (2010, 2011) and Goeijenbier et al. (2021). In particular, Oumeraci and Kortenhaus (1994) highlighted the importance of dynamic analysis for vertical breakwaters under impulsive wave loads, showing that when the length of the impulsive component (defined as the time interval encompassing the steep pressure rise followed by a sharp decay) exceeds the structure's natural period (commonly assumed to be the first mode), the response is amplified by dynamic effects. They also reported that for impulsive loads with durations less than 25% of the structure's natural period, the structural response is primarily controlled by the impulse magnitude (the time integral of the applied load) rather than by the temporal evolution of the loading.

Studies of structures with overhangs showed that upward impact forces increase on structures with overhangs and recurves. Prediction models, such as those by Ramkema (1978), Wood and Peregrine (1996), Kisacik et al. (2012), Kisacik et al. (2014) and Chen et al. (2019), De Almeida and Hofland (2020, 2021), verified that *pressure-impulse theory* applies effectively in assessing pressures on such structures.

According to Kortenhaus et al. (2004), curved crownwalls can significantly reduce overtopping; however, they also lead to an increase in wave loading by a factor of 1.1 to 1.8 as the loading shifts from non-impulsive to impulsive forces, compared to vertical breakwaters. Similarly, Pearson et al. (2005) conducted physical model tests on a vertical wall with a seaward-facing overhang/bullnose, revealing that the wave load was highly impulsive, with horizontal forces increased by a factor of 2 relative to a vertical wall. Large-scale experiments by Stagonas et al. (2014, 2020) and Ravindar et al. (2019) on breaking wave impacts against a vertical crownwall with a recurved crownwall indicated that both the exit angle and the overhang length contribute to an increase in wave load.

Castellino et al. (2018b) investigated large impulsive forces on recurved crownwalls under non-breaking wave conditions using Computational Fluid Dynamics (CFD) simulations. This study compared a recurved crownwall with a vertical wall of the same height, focusing on wave loadings. Results indicated a significant increase in wave pressure on the structure when the breakwater's crownwall was shaped as a recurve, leading to potential failure, as observed e.g. in Civitavecchia as shown in Fig. 1. Experimental studies support these findings (Martinelli et al., 2018), demonstrating that a larger exit angle of the recurved overhang results in a more significant load increase. The highest increase in force, compared to a vertical breakwater, occurs when the exit angle of the recurved crownwall reaches 90°. This phenomenon of up-rushing water being confined by a recurved overhang, leading to significant impulsive pressures affecting the entire breakwater, has been termed Confined-Crest Impact (C-CI) after Castellino et al. (2018b).

Dermentzoglou et al. (2020) conducted the first Finite Element (FE) analysis of the structural response of recurved crownwalls under C-CI loading focusing on the same crownwall as studied by Castellino et al. (2018b) and investigating the reasons for the possible structural failures. The study employed offline one-way coupling between the CFD-generated pressure time series from Castellino et al. (2018b) with a dynamic FE analysis. Results suggested that the crownwall may have been constructed using concrete with a strength class lower than C25/30, as structural analysis did not indicate failure under the estimated wave conditions ($H = 5$ m, $T = 8$ s) that were inferred as the cause of the Civitavecchia breakwater failure (Castellino et al., 2018b).

Despite extensive research on recurved crownwalls, the performance of fully curved crownwalls remains less understood, mainly when used atop vertical breakwaters. Fully curved crownwalls are commonly employed as seawalls in the UK (e.g., Scarborough, Fig. 1b) to reduce overtopping and withstand broken wave loads. Given this proven effectiveness in seawalls and their better hydraulic efficiency compared to recurved alternatives (Antonini et al., 2023), this paper primarily seeks to advance the understanding of the structural performance of recurved and fully recurved crownwalls by investigating the influence of their geometric characteristics under C-CI conditions. To achieve these objectives, a comparative numerical analysis is conducted. Structural behavior is evaluated using a FE method developed in DIANA FEA 10.5, where pressure time series derived from OpenFOAM simulations serve as primary loading conditions through an offline one-way coupling approach.

The structure of this paper is as follows. In Section 2, the two crownwall shapes are described, the CFD model is introduced as well as the adopted methodology for the structural analyses. In Sections 3 and 4, the results of the CFD simulations and structural analyses are presented. Section 5 includes a discussion of the main findings, while the final conclusions are given in Section 6.

2. Methods

2.1. Analyzed crownwall shapes

The geometries of the two crownwalls investigated are presented in Fig. 2, the recurved one and the fully curved, hereinafter referred

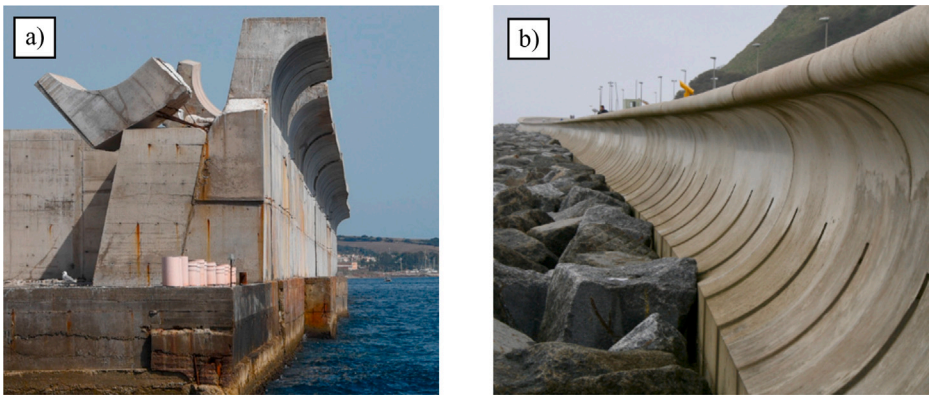

Fig. 1. (a) Failure of the recurved crownwall in Civitavecchia Harbour. (b) A fully curved crownwall on a rubble mound foundation as a part of a seawall structure in Scarborough, England (Castellino et al., 2021).

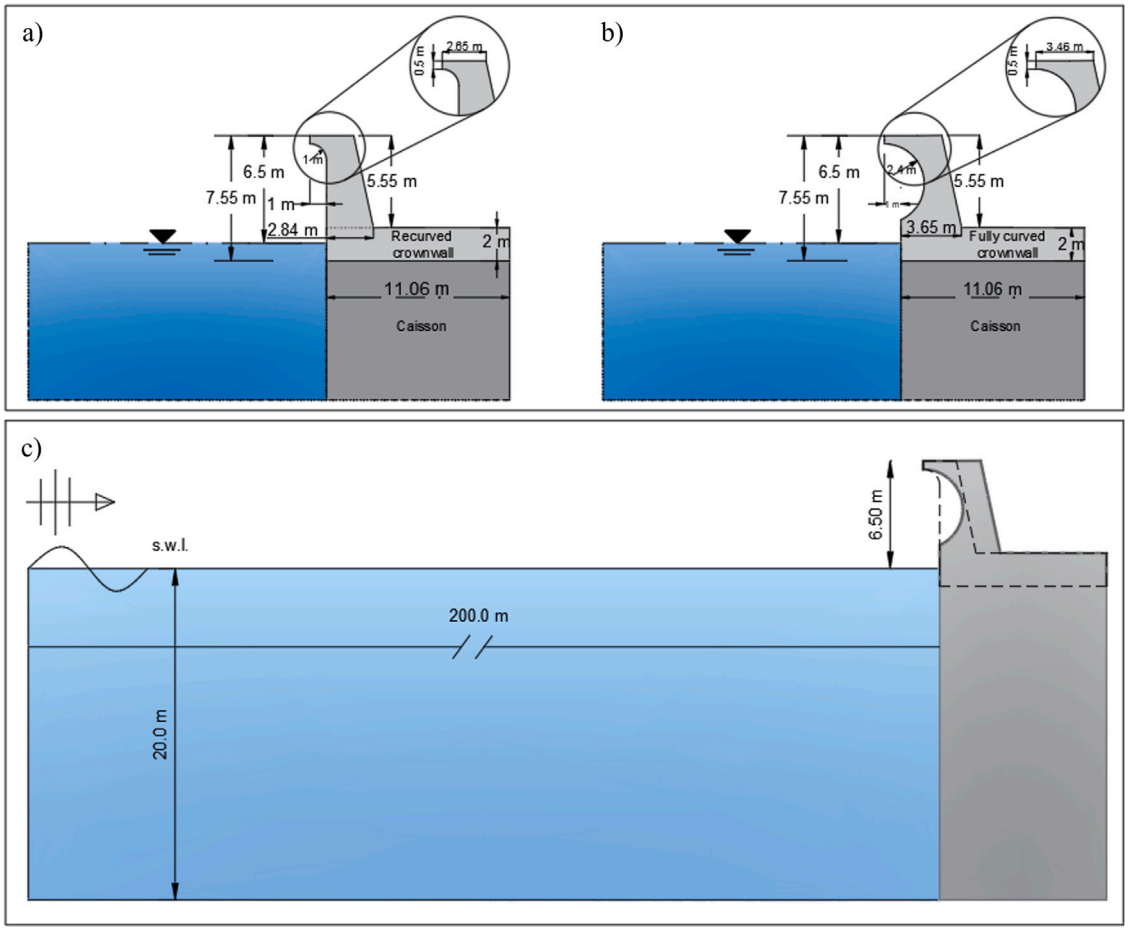

Fig. 2. Geometry of the R (a) and FC (b) crownwalls. In (c), the scheme of the numerical wave flume.

to as R and FC, respectively. The two shapes share a consistent cross-sectional area of 35 m^2/m, comprising a horizontal slab area of 22 m^2/m as already proposed by Dermentzoglou et al. (2020) (solid line area in Fig. 2c) and a vertical crownwall area of 13 m^2/m (dashed line area in Fig. 2c). As a result, both crownwall shapes are comparable in terms of the required amount of concrete. Key structural parameters, including the freeboard (R_c = 6.5 m), total height (7.55 m), and overhang length (B_r = 1 m), are consistent in both designs. However, the curvature radius of the FC crownwall is larger (1.4 m), and its cross-section at the narrowest point is smaller than at any section of the R crownwall, which may influence its structural response.

2.2. CFD model

The hydrodynamic simulations were conducted using IHFOAM (Higuera et al., 2013a,b), a specialized solver built on OpenFOAM® for coastal processes. The incompressible Reynolds-Averaged Navier–Stokes equations were solved, with the $k-\varepsilon$ turbulence model employed for closure. The free surface elevation is trucked using the Volume of Fluid (VOF) method (Hirt and Nichols, 1981) while the wave generation and active wave absorption is entrusted to IHFOAM numerical solver as already successfully employed by e.g. Higuera et al. (2014). Simulations are carried out at a prototype scale within a two-dimensional wave flume (200 m long, 40 m high as represented in Fig.

Table 1
Wave characteristics of numerically simulated wave conditions, where H is the wave height, T is the wave period, L_0 is the deep water wavelength, $s = H/L_0$ is the wave steepness, R_c/H is the relative freeboard, H/d is the wave height over water depth and d/L_0 is the water depth over wavelength.

Wave condition	H [m]	T [s]	L_0 [m]	s [%]	R_c/H [–]	H/d [–]	d/L_0 [–]
W5	5	8	100	5	1.30	0.25	0.20
W6	6	8	100	6	1.08	0.3	0.20
W7	7	11	189	3.7	0.92	0.35	0.11

2c), avoiding scale effects (Attili et al., 2023a). These conditions were selected based on the representative water depths typically observed along the Mediterranean coastal regions. Due to the high computational cost, the simulations were limited to regular waves only. As a result, only a small number of waves (around 15 zero-crossing waves) were modeled. This approach is supported by previous findings indicating that the peak loads on the structure typically occur during the early transient stage of the simulations. Further details on this approach are provided in Castellino et al. (2018b) and Castellino et al. (2018a). The three regular wave conditions selected for analysis, were previously identified by Castellino et al. (2018b) are W5, W6 and, W7, as inducing impulsive wave loads on R crownwalls. The integration time step is automatically chosen to ensure numerical stability. Nevertheless, the maximum time step allowed is fixed at 0.001 s in order to catch impulsive phenomena reached during the simulations. This aspect is critical due to the occurrence of impulsive pressures and forces over very short time scales. The Courant number was limited to a maximum value of 0.40 to ensure numerical stability.

Table 1 shows the selected conditions along with the wave height (H), wave period (T), deep water wavelength (L_0), wave steepness ($s = H/L_0$), relative freeboard (R_c/H), wave height over water depth (H/d) and water depth over wavelength (d/L_0). The water depth (d) in front of the crownwall is 20 m, and the seabed is assumed flat, representing typical conditions for vertical breakwaters along the Mediterranean coastline, e.g. in the harbor of Civitavecchia in Italy (Castellino et al., 2018b).

To ensure mesh-independent numerical results, a comprehensive grid convergence study was performed. The analysis was carried out for the R configuration subjected to regular wave conditions defined by a height of 5.0 m and a period of 8.0 s (test case $WR5$ in Table 1). The investigation involved multiple computational grids with varying spatial resolutions. An initial uniform mesh composed of square cells with $\Delta x = \Delta z = 0.50$ m was adopted based on the guidelines of Larsen et al. (2019). Subsequent simulations employed refined meshes with resolutions of $\Delta x = \Delta z = 0.30$ m, 0.25 m, and 0.15 m. The final grid adopted a non-uniform structure, featuring $\Delta x = 0.20$ m and $\Delta z = 0.15$ m, resulting in a vertical-to-horizontal spacing ratio of 0.75. To quantify the impact of mesh resolution on the numerical outcomes, the maximum pressure recorded at a fixed probe located on the R crownwall was selected as the reference metric, as previously carried out by Castellino et al. (2018b, 2021) and Castellino (2024).

A comprehensive numerical measurement campaign was conducted along the front faces of both the caisson and the crownwalls. A total of 154 and 131 measuring probes are used for the FC and R crownwalls, respectively, recording pressure for at least 7 incoming waves. In the vertical part of the breakwater the probes are spaced at intervals of 0.25 m below the still water level (SWL), and 0.1 m above the SWL. On the curved parts of the crownwalls, a probe is located at every 5° as shown in Fig. 3. As only the crownwalls are modeled in the FE model, only the top 79 and 56 probes are considered for the R and FC, respectively.

2.3. Wave impact types and loading domain

Two classification approaches are commonly used to analyze impulsive wave loading on structures. The first focuses exclusively on the nature of the impulsive load (Kortenhaus and Oumeraci, 1998), while the second considers the impulsive load in relation to the dynamic response of the structures (Oumeraci and Kortenhaus, 1994).

Table 2
Pressure impact types (Huang et al., 2022) and loading domains (Chen et al., 2019).

Impact type Loading domain	P_{Im}/P_{qs+}	T_d/T_n
Quasi-static	< 1.2	≥ 4
Dynamic	1.2 – 2.5	0.25 – 4
Impulsive	> 2.5	< 0.25

Fig. 4 illustrates the pressure time series for the largest modeled wave height (i.e. W7) recorded at probes 70 and 47 for the R and FC crownwalls, respectively. This time series exhibits the characteristic "church roof" profile, consisting of a maximum impulsive pressure (P_{Im}) followed by a gradually varying quasi-static peak (P_{qs+}). The impact classification framework, originally proposed by Kortenhaus and Oumeraci (1998) and later refined by Streicher et al. (2019) and Huang et al. (2022), categorizes impacts into three types: quasi-static, dynamic, and impulsive. This categorization is based on the ratio P_{Im}/P_{qs+}, as shown in the first column of Table 2. While this approach provides a general understanding of the impact type, a more detailed evaluation of the wave loading domain is required to account for the interaction between the wave-induced forces and the structure's dynamic behavior (Antonini et al., 2021). The framework proposed by Oumeraci and Kortenhaus (1994) and refined by Humar (2012) and Chen et al. (2019) evaluates this aspect by comparing the impulse duration (T_d) with the structural natural period (T_n). Table 2 summarizes the thresholds proposed by Chen et al. (2019) to distinguish the different domains. In this study, the natural period (T_n) is associated with the first bending mode, as it dominates during the wave loading phase. The impulse duration (T_d) is determined manually by analyzing the pressure time series and its first derivative, which supports the definition of the start (t_a) and end (t_b) of the impulse by suggesting sharp changes. The impulse duration (T_d) is determined manually by analyzing the pressure time series and its first derivative, which supports the identification of the start (t_a) and end (t_b) of the impulse by highlighting sharp changes in the signal. This approach is motivated by the lack of a universally accepted and quantitatively unambiguous definition of impulse duration. As such, we adopted a manual procedure, in which the first derivative proved particularly helpful in identifying the steep pressure rise typically associated with impulsive loading, as described by Oumeraci and Kortenhaus (1994). The resulting pressure (or force) impulse, I_P (or I_F), is then computed by integrating the pressure (or force) time series over this duration.

2.4. Static stress analysis

Static linear analysis is performed through simplified analytical formulations to preliminary estimate the internal stress of the two crownwalls due to the wave load. For various cross-sections along the crownwalls height above the horizontal slab, the total bending moment, M_{tot}, and the total vertical force, $F_{V,tot}$, are determined at the instant of maximum total force of the largest wave for each simulated wave condition. The largest wave of each wave condition is defined as the

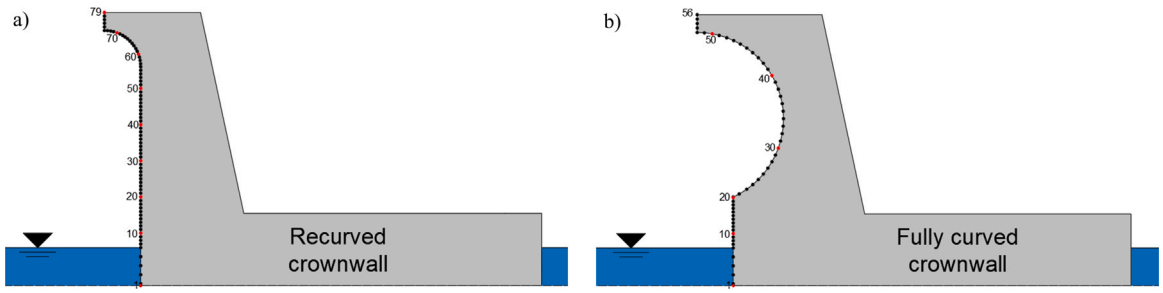

Fig. 3. Measuring probes along the "(a)" R and "(b)" FC crownwalls. The probes are numbered such that probe 1 is located at the bottom of the crownwall and probes 79 and 56 at the top.

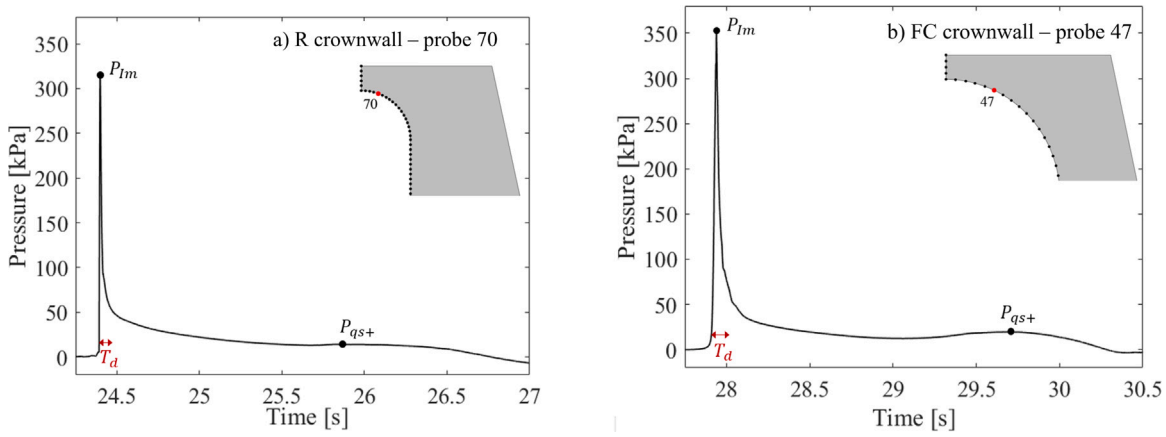

Fig. 4. Pressure time series of the largest wave of W7 at probes 70 and 47 on the R and FC crownwall in (a) and (b) respectively. Maximum impact pressure, P_{Im}, maximum quasi-static pressure, P_{qs+}, and impulse duration, T_d, are indicated.

wave that exerts the largest total force on the crownwalls. Fig. 5 shows an example of the forces acting on different cross-sections for both R and FC crownwalls. The maximum total wave forces, acting within each wave condition, are decomposed into horizontal and vertical forces, F_H and F_V. These wave forces contribute to a bending moment acting clockwise, creating tension in the front face of the crownwall and compression in the back face. The self-weight (SW) of the crownwalls above the analyzed cross-section acts as a downward vertical force, generating an anti-clockwise bending moment that partially counteracts the wave-induced bending moment. The bending moment of each force is calculated with reference to the center of the cross-section, shown as a red dot in Fig. 5. Once the overall loading condition has been determined, Eq. (1) is used to calculate the stresses in the y-direction in Fig. 5, where the bending moment is M_{tot}, and I_{zz} is the second moment of area defined as $I_{zz} = b^3 \cdot h/12$, with A representing the cross-sectional area. All the involved parameters, b, x, I_{zz}, A, and M_{tot}, are height-dependent. In particular, M_{tot} and $F_{V,tot}$ vary due to the changing of the cross section along its height, while $A = b \cdot h$ also varies since b (the local width at specific height) changes and h (the out-of-plane unit width) is constant and equal to 1. To determine the maximum tensile stress in the crownwall ($\sigma_{t,yy,\max}$), the distance between the center of each cross-section and its front face is defined as $x = b/2$. The stresses are then calculated as:

$$\sigma_{t,yy,\max} = \frac{M_{tot} \cdot x}{I_{zz}} + \frac{F_{V,tot}}{A} \tag{1}$$

2.5. Finite element model

The crownwalls are modeled in 2D on the xy plane using plane-strain elements adopting a quadrangle/hexahedron mesh. The structural analysis considers normally incident waves; hence, wave obliqueness, crownwall length and out-of-plane strain components, as well as deformation, are considered negligible. The crownwalls are assumed to be constructed on a concrete caisson, with the interface modeled as fully rigid so that sliding and overturning are not allowed, which might slightly increase the calculated internal stresses. Reinforcement bars are excluded from the model, enabling the identification of tensile stress concentrations through linear analysis. Nonlinear analysis is also performed to evaluate crack formation in cases where tensile stresses exceed the concrete's strength.

According to Eurocode 2 (E.N. 1992-1-1, 2004), the concrete crownwalls belong to exposure class XS3 (tidal, splash, and spray zones) and should, therefore, be constructed with a concrete strength class at least equal to C35/45. The Young's modulus for this strength class is E = 34 GPa (EN1992-1-1, 2004), the mean tensile strength is $f_{ctm} = 3.2$ MPa and the mean compressive strength is $f_{cm} = 43$ MPa. The mass density of concrete is taken as $\rho = 2400\ \text{kg/m}^3$ and the Poisson's ratio as $\nu = 0.2$.

A total strain-based crack model is used as a cracking model for the nonlinear analysis. This constitutive model is based on the Modified Compression-Field Theory (Vecchio and Collins, 1986) and its 3D extension proposed by Selby (1994). The model employs a smeared crack approach, where cracks are represented as distributed effects over a specific area. This approach assumes that the cracked material remains continuous, enabling the tensile and compressive behavior to be characterized through a stress–strain relationship. The model adopts a rotating crack approach, evaluating the stress–strain relationship within a coordinate system that aligns with the principal strain direction. This allows the crack orientation to evolve dynamically, eliminating the need for shear retention assumptions (Rots, 1991; Naeimi and Moustafa, 2017; DIANA FEA BV, 2021). The compressive behavior of the concrete is defined based on the compression curve specified in Eurocode 2 for concrete class C35/45. For the tensile behavior, the model employs a linear tension-softening curve derived from the fracture energy defined as the energy absorbed per unit area of the crack as it forms (Słowik, 2019).

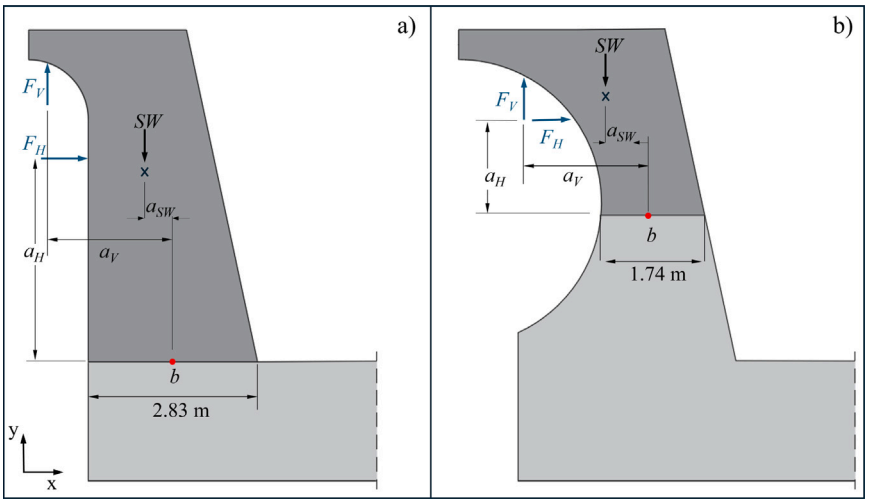

Fig. 5. Points of application of the horizontal and vertical wave forces, F_H and F_V, and the self-weight of the crownwall, SW, acting on the most critical cross-sections of the "(a)" R and "(b)" FC crownwalls. The bending moment arms a_H, a_V, and a_{SW} and the widths of the cross-sections, b, are also presented.

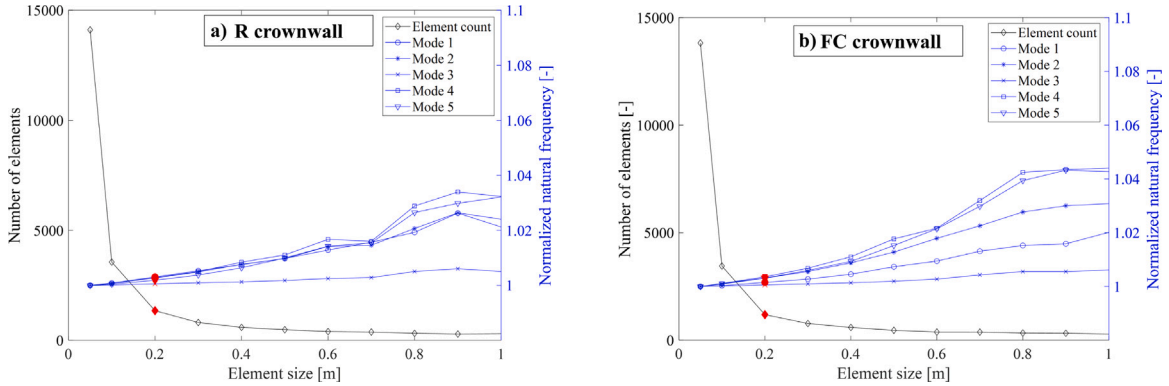

Fig. 6. Results of FEM mesh sensitivity analysis. A mesh size of 0.2 m is chosen, shown in red markers, with regard to the convergence of the eigenfrequencies and the number of elements.

A mesh sensitivity analysis is performed to determine the optimal mesh size for the FEM model of the structure alone, without considering fluid–structure interaction or the presence of water. The first five eigen-frequencies are used to evaluate the model convergence, as shown in Fig. 6a (R crownwall) and in Fig. 6b (FC crownwall). The right y-axis (blue) presents eigenfrequencies normalized against those obtained with the most refined mesh (i.e. 0.05 m). Minimal changes in eigenfrequencies were observed for mesh sizes below 0.2 m, with the smallest tested size (0.05 m) differing by only (~ 1%–5%) from the 1 m mesh results. The left y-axis (black) indicates the number of elements for each mesh size, providing an indirect measure of computational cost. A mesh size of 0.2 m was selected as the best compromise between eigenfrequency convergence and computational efficiency.

3. Results of CFD simulations

The results of the CFD simulations are presented in terms of pressures (P) and forces (F), while the relative effectiveness in reducing wave overtopping is proposed by contrasting the individual overtopping volume (V) measured for the three regular wave conditions for both crownwall shapes.

3.1. Pressure field

The pressure distributions along the R and FC crownwalls under the simulated wave conditions exhibit distinct patterns influenced by their geometries. Fig. 7 illustrates the non-dimensional pressure distributions along the vertical sections of both crownwalls. These distributions are expressed as the ratio of pressure on the crownwalls to that on a vertical wall of the same height, evaluated at the moment of the maximum total force. For the R crownwall, the non-dimensional pressure increases consistently with height, starting from the still water level. A steeper gradient is observed as the pressure approaches the beginning of the recurved section, highlighting the increased pressure due to the C-CI effect. In contrast, the FC crownwall exhibits a more uniform pressure gradient, with the pressure increase beginning at the base of the recurve and influencing the entire height of the wall. Overall the FC crownwall experiences higher pressures and longer impulses along its entire height imposing greater structural demands compared to the R crownwall.

The maximum pressure (P_{max}) and pressure impulse (I_P) recorded at probes 70 and 47 (see Fig. 4) corresponding to the P_{max} locations are summarized in Table 3. The pressure impulses are negatively correlated with the wave steepness (s). Steeper waves, with higher vertical accelerations (a_w), lead to shorter impulse durations. In contrast, the maximum pressure (P_{max}) is positively correlated with the wave height (H). This opposing behavior in contributing to the pressure impulse is further amplified by the FC geometry, which, unlike the R crownwall, facilitates fluid detachment from the wall. In the extreme case of wave condition W6 — the steepest among those tested — the fluid completely detaches from the wall, leading to the wave crest slamming onto the upper part of the structure, producing the shortest and smallest impulse acting on the FC crownwall.

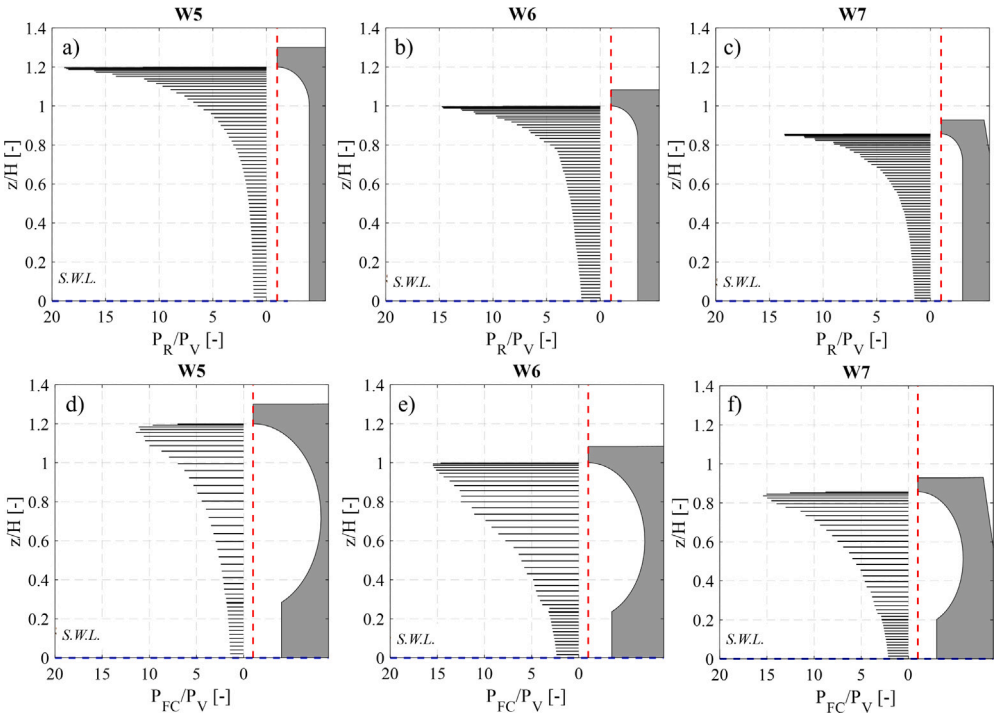

Fig. 7. Comparison between the non-dimensional pressure distribution along the vertical sections of the R (a), (b), and (c) and FC (d), (e), and (f) crownwall.

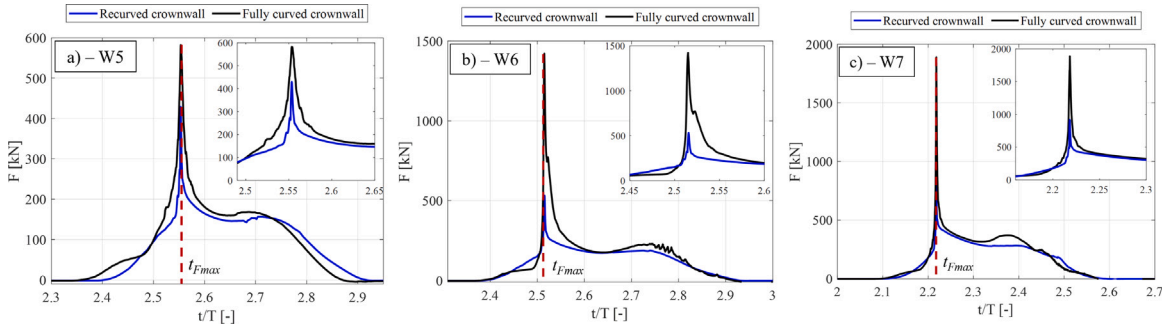

Fig. 8. Time series for the maximum total force acting on the R (blue) and FC (black) crownwalls for (a) wave state W5, (b) W6 and (c) W7.

3.2. Forces

The wave pressure field is geometrically integrated to compute the wave forces acting on the structures. The resulting time series are presented in Fig. 8 for both crownwall geometries, focusing on the event generating the maximum total force for each tested wave condition, where the maximum total force refers to the overall resultant force magnitude. The force acting on the FC crownwall gradually increases with the rising water surface. Upon reaching the bottom of the curve, the force gradient sharply intensifies, leading to a peak characteristic of an impulsive force indicated in Fig. 8 with t_{Fmax} at the dimensionless time (t/T) 2.55; 2.50 and 2.20, respectively for W5, W6 and W7.

However, the force acting on the R crownwall steadily increases until the water surface reaches the tip at the crownwall's summit, at which point the force becomes impulsive. Notably, a significant distinction between the two shapes lies in the duration of this impulsive force component, which consistently remains longer for the force acting on the FC crownwall. Table 3 presents the wave height and period for the three simulated conditions, along with the maximum pressure, pressure impulse, maximum total force, and the corresponding force impulse. All maximum force and pressure values are classified as impulsive according to the criterion proposed by Huang et al. (2022), as shown in the second column of Table 2. The maximum total force acting on the FC crownwall is 1.35, 2.5, and 2 times greater than that on the R crownwall for W5, W6, and W7, respectively. Similarly, the difference in force impulses between the two crownwalls exceeds the difference in pressure impulses, underscoring the critical influence of the FC crownwall's larger surface area.

3.3. Overtopping

To provide an initial assessment of the relative hydraulic efficiency of the two shapes, we analyze individual overtopping events generated under the same impulsive conditions used to determine the maximum total force. Overtopping volumes are measured at an interface located on the seaward side, at the top of each crownwall. For each wave condition, the maximum volume recorded for the vertical wall is used as a reference to quantify the reduction rate due to the investigated structure. As illustrated in Fig. 9, when the relative freeboard is lower than one, both shapes exhibit similar behavior, with overtopping volumes predominantly determined by the wave crest passing directly over the crownwall. However, at relative freeboard values just above unity, the FC crownwall yields a more pronounced reduction in overtopping volume. As the relative freeboard increases further, the differences between the two shapes become negligible, and both effectively redirect the incident wave offshore. Although this suggests a potential optimal

Table 3
Wave conditions characteristics: wave height (H), wave period (T), wave steepness (s), maximum linear horizontal (u) and vertical (w) orbital velocity, maximum linear horizontal (a_u) and vertical (a_w) orbital accelerations, maximum pressure (P_{max}), pressure impulse (I_P), maximum total force (F_{max}), and force impulse (I_F).

Crownwall	Wave condition	H [m]	T [s]	s [%]	u [m/s]	w [m/s]	a_u [m/s^2]	a_w [m/s^2]	P_{max} [kPa]	I_P [kPa s]	F_{max} [kN/m]	I_F [kN s/m]
R	W5	5	8	5.6	2.21	1.96	1.74	1.54	135	2.8	430	10
	W6	6	8	6.7	2.65	2.36	2.08	1.85	185	3.2	560	11
	W7	7	11	5.1	2.76	2.00	1.58	1.14	315	5.0	915	16
FC	W5	5	8	5.6	2.21	1.96	1.74	1.54	90	5.9	580	34
	W6	6	8	6.7	2.65	2.36	2.08	1.85	220	4.7	1420	81
	W7	7	11	5.1	2.76	2.00	1.58	1.14	360	8.5	1890	62

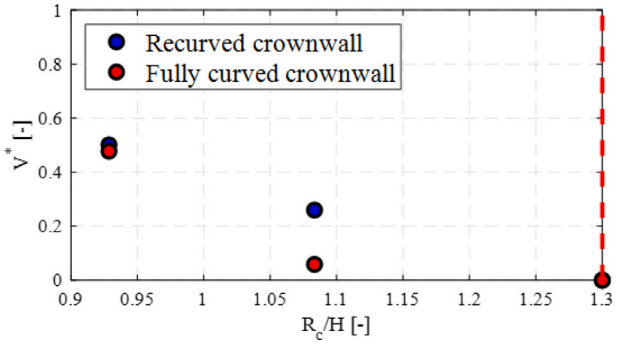

Fig. 9. Non-dimensional individual overtopping volumes.

range for the FC crownwall, identifying such a range is beyond the scope of this study.

4. Results of structural analysis

4.1. Static analysis

The static analysis investigates the distribution stress within the critical cross-sections of both crownwall geometries under the action of the pressure distribution at the moment of the maximum wave force (see Fig. 10). For the R crownwall, the stress is highest in the section just above the slab, where the bending moment (M_{tot}) reaches its peak. In contrast, the narrower cross-section of the FC crownwall, approximately 1.1 m smaller than that of the R crownwall, significantly amplifies the tensile stresses in the FC design. The maximum tensile stresses are observed near the center of its curve, which coincides with its narrowest cross-section. Analytical (Section 2.4) and FE (Section 2.5) approaches are employed. The analysis reveals that the bending moment is dominant in determining the stress distribution in both structures. For wave conditions W6 and W7, the stress exceeds the tensile strength of the C35/45 concrete class, i.e. f_{ctm} = 3.2 MPa, suggesting that cracking is likely possible under these conditions. Both confirm the locations of maximum tensile stress, occurring at probe 16 for the R crownwall (about 2.1 m above the SWL) and probe 33 for the FC crownwall (about 4.4 m above the SWL). While the R crownwall exhibits relatively linear stress distributions, the FC crownwall shows non-linear stress behavior, with higher tensile stress gradients on the front face. The comparison between analytical and FE results showed good agreement for the R crownwall, with analytical calculations overestimating stresses by approximately 7%. However, for the FC crownwall, analytical methods underestimated the stresses by 20%, underscoring the importance of accounting for non-linearities in curved geometries. The results of the two approaches are reported in Table 4. (see Fig. 11).

4.2. Modal analysis

The modal analysis examines the dynamic properties of the two crownwalls to determine their response under wave-induced loading. Despite their different geometries, both crownwalls exhibit similar first eigenmodes, reflecting comparable dynamic behavior in the vertical portion of the structures. The recurved crownwall, with its wider critical cross-section, shows slightly higher stiffness, resulting in marginally higher eigenfrequencies. The cumulative modal mass confirms that the first six modes capture approximately 80% of the total structural mass for both shapes (Table 5). The first two modes are particularly influential, as they dominate the response of the vertical part of the crownwalls (Figs. 12). Higher-order modes either minimally contribute to the dynamic response or mainly affect the horizontal slab rather than the vertical part (Figs. 13). These modes are less significant for the crownwall's dynamic response to wave action because wave loads predominantly act on the vertical part of the structures. Consequently, the response of the slab has minimal impact on the critical stress distributions observed in the crownwalls.

4.3. Wave impact types and loading domain

The classification approaches for impact types and loading domains are applied to four probes located within the top 2–2.5 m of each crownwall (Fig. 14), based on the time series generated by the wave producing the maximum force in each wave condition. In this upper region, all pressure impacts are classified as impulsive, according to the criteria outlined in the second column of Table 2. Below this region — at distances greater than 2.5 m from the crownwall's top — impacts on the R crownwall for all wave conditions and on the FC crownwall under W5 are categorized as dynamic. In contrast, for the FC crownwall under wave conditions W6, and W7, this lower region is predominantly characterized by impulsive impacts, with only a small area around the mean sea level exhibiting dynamic behavior.

Following the criteria outlined in the third column of Table 2, the definition of the loading domain requires the comparison between the impulse durations and the natural period, in this case the one relative to the first mode, i.e. $T_{n,R}$ = 0.028 s and $T_{n,FC}$ = 0.031 s. The identified impulse durations are shown in Fig. 14, in which circles represent the impulses acting on the R crownwall, and diamonds represent those acting on the FC crownwall. The four probes analyzed are marked as blue and black dots on the front faces of the R and FC crownwalls, respectively. The minimum impulse durations for the dynamic loading domain are $T_{d,R}$ = 0.11 s for the R and $T_{d,FC}$ = 0.12 s for the FC crownwall. These thresholds are represented in Fig. 14 by dashed lines, blue for the R crownwall and black for the FC crownwall. For the R crownwall, all the impulse durations at the analyzed probes fall within the dynamic loading domain. For the FC crownwall under W7, the impulse durations fall entirely within the dynamic domain. Under W6, dynamic impulses are recorded only at the upper two probes, while the lower two remain in the quasi-static domain. All impulses from W5 acting on the FC crownwall fall within the quasi-static domain. None of the pressure impulses reach the impulsive loading domain, underscoring the necessity of dynamic structural analysis for both crownwalls under most wave conditions.

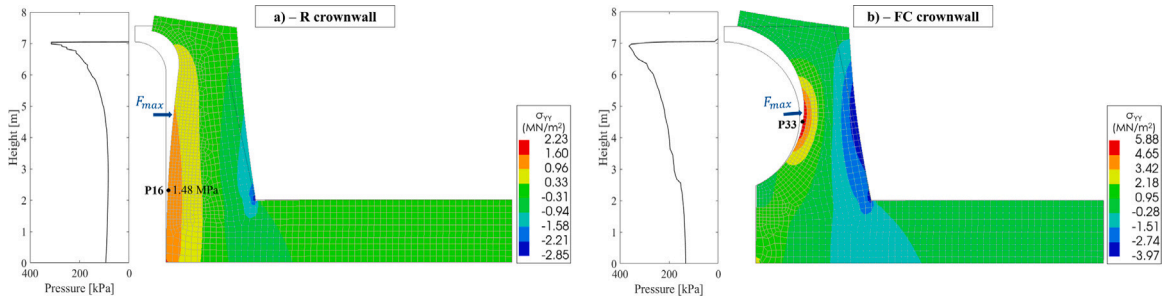

Fig. 10. Static FE analysis for W7 showing the pressure distribution along the crownwall height at the moment of maximum wave force and the corresponding stress distribution in y-direction. The blue arrow indicates F_{max}, and the black dot marks the location of maximum tensile stress.

Table 4
Bending moment (M_{tot}) acting on the critical cross-sections, results of analytical calculations of maximum tensile stresses ($\sigma_{t,yy,max}$), results of static FEA in Diana ($\sigma_{t,yy,max}$) and the difference in the results of the two methods.

Shape	Wave condition	M_{tot} [kNm/m]	$\sigma_{t,yy,max}$ [MPa] Analytical	$\sigma_{t,yy,max}$ [MPa] Static FEA	Analytical/Static FEA
R	W5	870	0.58	0.54	1.07
	W6	1245	0.87	0.81	1.07
	W7	2150	1.59	1.48	1.07
FC	W5	495	0.98	1.19	0.83
	W6	1490	3.11	3.80	0.82
	W7	2270	4.78	5.88	0.81

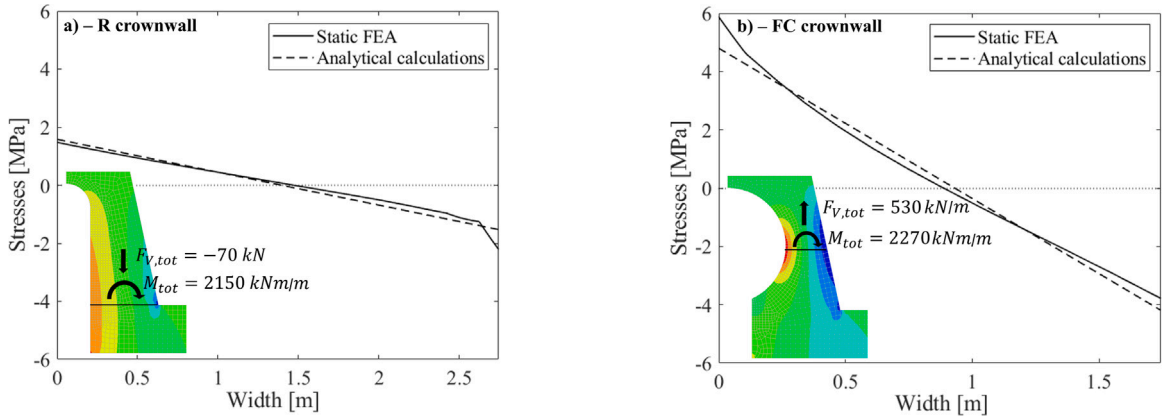

Fig. 11. Vertical stress distributions (σ_{YY}) in the critical cross-sections of the two crownwalls under wave load from the largest wave in W7. The total vertical force ($F_{V,tot}$) and total bending moment (M_{tot}) of W7 acting on the cross-sections are presented.

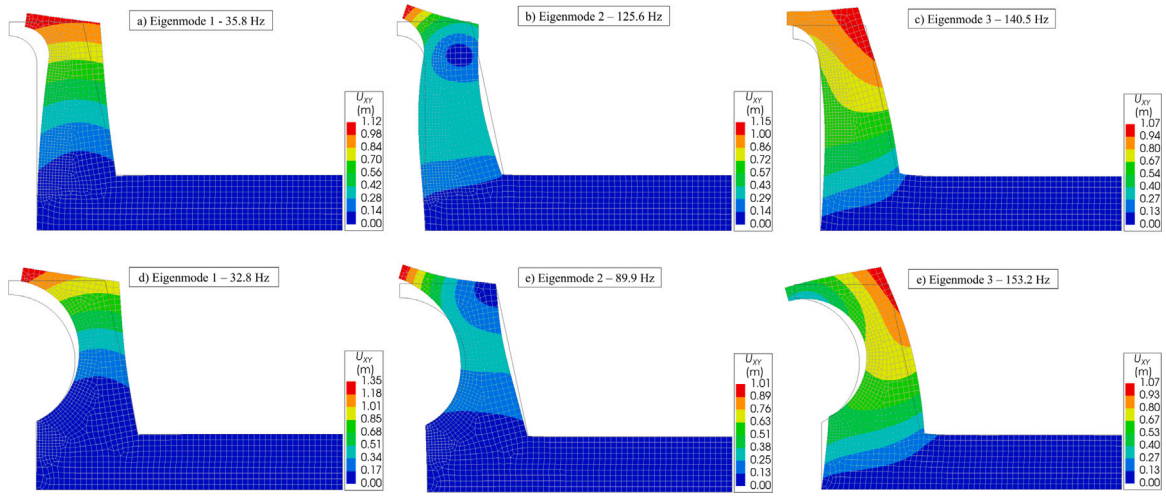

Fig. 12. The first three eigenmodes of the (a), (b), and (c) R and (d), (e) and (f) FC crownwalls. The color scale represents the magnitude of the displacement.

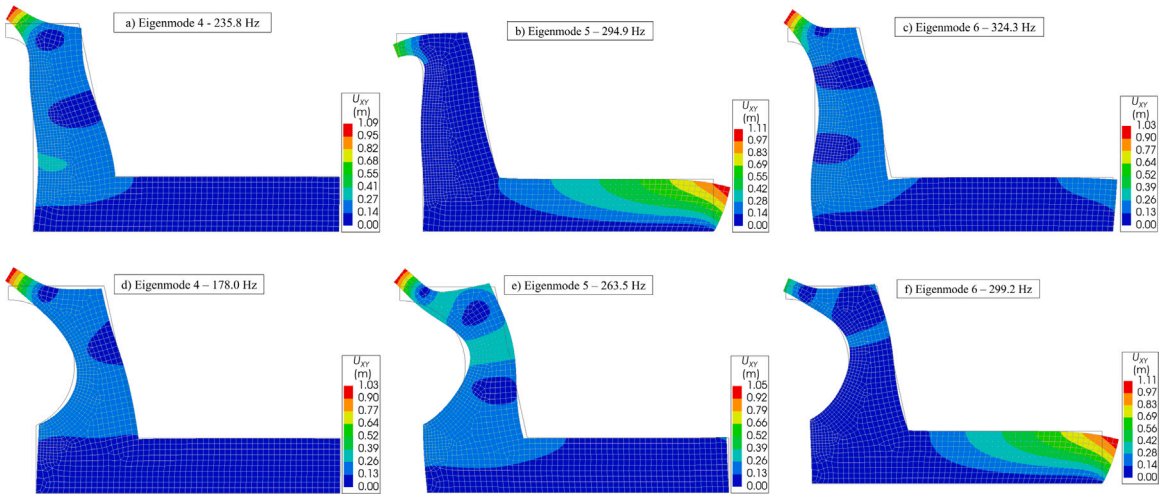

Fig. 13. Eigenmodes 4–6 of the (a), (b), and (c) R and (d), (e) and (f) FC crownwalls. The color scale represents the magnitude of the displacement.

Table 5
Effective modal mass in the global x-direction of the first five to six eigenmodes of the two crownwalls.

Shape	Eigenfrequency [Hz]	Effective mass [kg]	Mass percentage [%]	Cumulative mass percentage [%]
Recurved	35.8	22 085	26.1	26.1
	125.6	12 933	15.3	41.3
	140.5	106	0.1	41.4
	235.8	10 871	12.8	54.3
	294.9	22 466	26.5	80.8
	324.3	566	0.7	81.4
Fully curved	32.8	15 647	18.4	18.4
	89.1	11 944	14.1	32.5
	153.2	4716	5.6	38.1
	178.0	7998	9.4	47.5
	263.5	13 242	15.6	63.1
	299.2	14 635	17.2	80.3

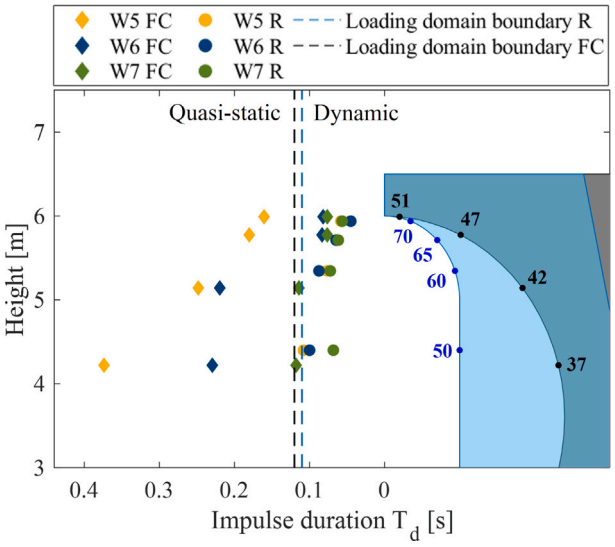

Fig. 14. Impulse duration, T_d, of pressure impulses of the largest wave of each wave, state acting on the top of the two crownwalls. Pressure impulses acting on the R crownwall are shown as diamonds and those acting on the FC crownwall are shown as circles.

4.4. Dynamic structural analysis

Rayleigh damping is used in the dynamic analysis of the crownwalls to define the damping matrix ($\bar{C}$), expressed as a linear combination of the mass ($\bar{M}$) and stiffness ($\bar{K}$) matrices: $\bar{C} = \alpha\bar{M} + \beta\bar{K}$ where α and β are Rayleigh damping coefficients. These coefficients are defined by specifying a damping ratio, $\zeta_n = 5\%$, at two frequencies: $f_1 = 35$ Hz, which is close to the natural frequency of the first mode for both structures, and $f_2 = 890$ Hz and 895 Hz for the R and FC crownwalls, respectively. The latter frequencies correspond to the point where the cumulative effective modal mass reaches 90% of the total mass. This results in Rayleigh damping coefficients $\alpha_R = 15.08$ 1/s and $\beta_R = 1.74 \cdot 10^{-5}$ s for the R crownwall and $\alpha_{FC} = 15.28$ and $\beta_{FC} = 1.73 \cdot 10^{-5}$ for the FC crownwall.

4.4.1. Linear dynamic analysis

Dynamic linear analysis is performed for the R and FC crownwalls under the three tested wave conditions. The pressure time series generated by the wave producing the maximum force in each wave condition is used to drive the FE model. Maximum compressive stresses remained below the concrete's compressive strength for both designs. However, tensile stresses in the FC crownwall exceeded the tensile strength for W6 and W7, indicating potential cracking. Dynamic effects were assessed using the Dynamic Amplification Factor (DAF), defined as the ratio of the maximum tensile stress ($\sigma_{t,yy,max}$) in the dynamic analysis to that in the static FEA presented in Table 4. The results demonstrate that dynamic effects amplified stresses, with DAF values consistently exceeding unity, as shown in the last column of Table 6.

Stress distributions reveal that maximum tensile stresses occur near the base of the R crownwall and at the curve's center for the FC crownwall, consistent with static analysis findings. The FC crownwall experiences higher stress concentrations due to its narrower critical cross-section. Displacement patterns and stress contours in Fig. 15

Table 6
Maximum compressive (σ_c) and tensile (σ_t) stresses in x- and y-directions.

Shape	Wave condition	$\sigma_{c,xx,max}$ [MPa]	$\sigma_{t,xx,max}$ [MPa]	$\sigma_{c,yy,max}$ [MPa]	$\sigma_{t,yy,max}$ [MPa]	DAF [−]
R	W5	−1.48	0.29	−1.72	0.78	1.4
	W6	−1.81	0.37	−2.09	0.98	1.2
	W7	−2.93	0.65	−3.38	1.78	1.2
FC	W5	−0.98	0.31	−1.24	1.34	1.1
	W6	−3.05	1.18	−3.85	5.04	1.3
	W7	−3.90	1.61	−4.99	7.20	1.2

align with the modal shapes, with dynamic effects predominantly governed by the first eigenmode. While the FC crownwall responds quasi-statically under W5, dynamic responses are observed for W6 and W7, as impulses duration fall within the dynamic loading domain resulting in larger DAF values in Table 6. Fig. 15 also highlights the differences in pressure distribution between the two crownwalls during the conditions of maximum total force and maximum stresses, i.e. also, maximum displacement. For the R crownwall, the maximum displacement and tensile stresses occur slightly after the wave pressure begins to decrease, indicating a time lag of a few ms between the peak force and the peak structural response. In contrast, the FC crownwall maximum stress is nearly synchronous with the maximum force, emphasizing a more immediate response to the applied loading. The temporal evolution of stresses at probes 16 (R crownwall,) and 33 (FC crownwall, Figs. 16d–f) — the locations of maximum tensile stresses — is shown in Fig. 16, along with the wave pressures at these locations and at the tops of the crownwalls (dashed and solid lines, respectively). For both crownwalls, tensile stresses begin to develop only when the wave impacts the top of the curve, initiating the pressure impulse. The R crownwall, Figs. 16a–c, exhibits a consistent dynamic response across all wave conditions, with oscillations occurring as the wave pressure diminishes. In contrast, the FC crownwall (Figs. 16d–f) responds quasi-statically under W5, with only minor stress oscillations during pressure reduction. However, under W6 and W7, the FC crownwall transitions to a dynamic response. Under W6, the behavior of the FC crownwall differs notably, as the maximum pressure is concentrated just above the center of the recurve. This localized pressure remains elevated even after the pressure impulse ends (Fig. 16), causing tensile stresses to oscillate for an extended period before gradually transitioning to compression. The tensile strength of the concrete (f_{ctm} = 3.2 MPa) is exceeded in the FC crownwall under W6 and W7, identifying these cases as suitable for non-linear analysis.

4.4.2. Nonlinear dynamic analysis

Fig. 18 presents contour plots at the moment of the maximum crack widths, indicated by the black cross in the time series shown in Fig. 17. Initial cracks form on the front face of the crownwall at the locations of maximum tensile stresses and propagate through the entire cross-section, ultimately leading to structural failure. For W6, a single crack propagates through the cross-section, whereas for W7, the presence of two cracks reflects the influence of higher wave pressures and the steeper pressure gradient at the crownwall's top. The maximum crack widths on the front face are substantial, reaching 29 mm for W6 and 55 mm for W7. At the moment of maximum cracking, the wave pressure has significantly diminished while the application point of the resulting force lies in the lower half of the crownwall's curved profile. The location and evolution of the cracks are not solely governed by the external pressure distribution shown in Fig. 7, but also by the internal stress patterns arising from the cross-sectional geometry. In particular, the cracks align with the zones of maximum tensile stress identified in the linear static (Fig. 10) and dynamic (Fig. 15) analyses. This consistency highlights the importance of both external loads and internal stress redistribution in driving failure. Overall, these findings underscore the structural vulnerability of the FC crownwall to impulsive wave loading and suggest that additional bar reinforcement may be necessary to enhance its resilience.

5. Discussion

The present study adopts a one-way coupling approach, assuming that structural deformations remain small. This simplification, commonly accepted for massive coastal structures such as crownwalls, generally leads to conservative force estimates, as rigid bodies typically experience higher impact forces than flexible ones (Attili et al., 2023b). The absence of fluid–structure interaction neglects the added mass effect introduced by the surrounding water, which would likely increase the natural periods of the system (Oumeraci and Kortenhaus, 1994). Although this may slightly reduce peak stresses in a fully coupled model, it is not expected to significantly affect the failure modes identified in this study.

The geometry of crownwalls significantly affects their response to wave-induced loading. The FC crownwall is subjected to higher total wave forces compared to the R crownwall, due to its larger radius and continuous curvature, which result in a gradual increase in wave pressure along the structure's height. The R crownwall, however, experiences a sharper pressure peak at its top due to the C-CI phenomenon, while the FC crownwall exhibits larger and more uniform pressure distribution along its height, leading to greater overall loading.

Dynamic analyses reveal that the FC crownwall experiences tensile stresses 1.7 to 5.1 times higher than those in the R crownwall across the tested wave conditions. This difference is primarily due to the narrower critical cross-section of the FC crownwall and its non-linear stress distribution concentrated at the curve's center. This structural vulnerability requires significant reinforcement to prevent cracking under extreme wave conditions. In contrast, the R crownwall's wider cross-section and linear stress distribution contribute to better structural performance. The duration of wave pressure impulses significantly influences the dynamic response of both crownwalls. Longer impulses, as observed for the FC crownwall, tend to align more closely with the structure's natural frequencies, potentially amplifying stress oscillations and dynamic effects. In contrast, the R crownwall, subjected to generally shorter impulse durations, exhibits a comparatively smaller dynamic amplification of internal stresses.

From a practical perspective, the FC crownwall offers some improvement in reducing overtopping volumes; however, this comes with significantly higher reinforcement requirements, leading to increased construction costs and a larger carbon footprint. Whether these structural drawbacks outweigh the potential hydraulic benefits remains uncertain and is likely to depend on project-specific considerations. However, they represent important factors that should be carefully evaluated in the design process. This trade-off between hydraulic and structural performance highlights the importance of an integrated design approach, where a detailed understanding of the interaction between wave-induced loading and structural response is valuable for optimizing performance and enhancing durability under extreme conditions.

6. Conclusions

This study compares the preliminary hydraulic and structural performance of recurved (R) and fully curved (FC) crownwalls under impulsive wave loads due to non-breaking waves, using a one-way

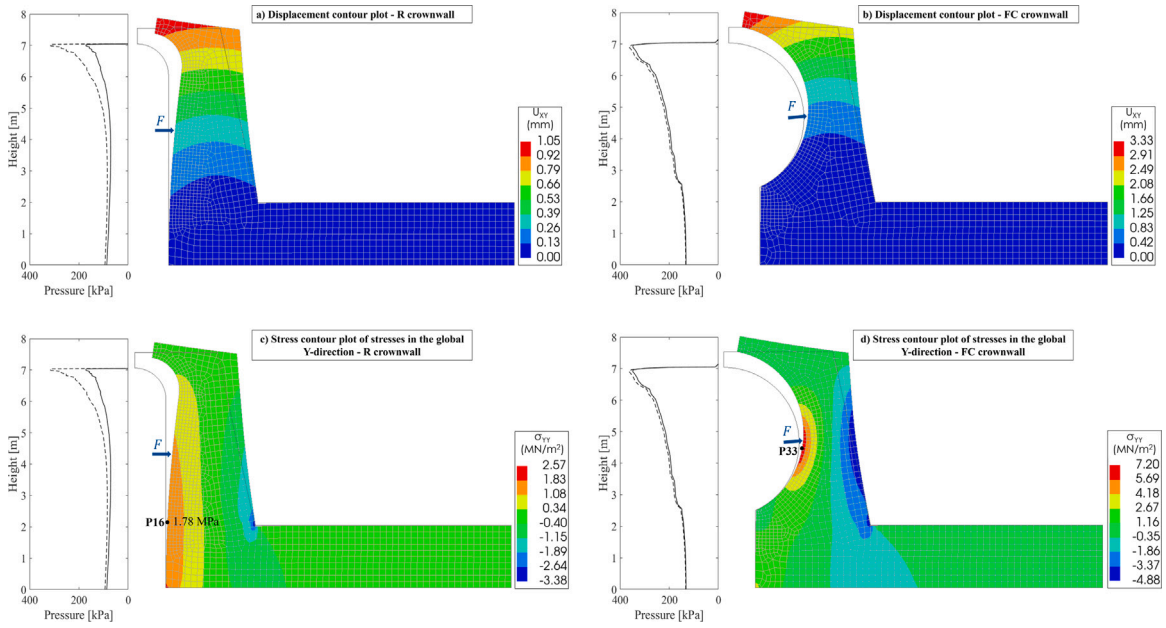

Fig. 15. Dynamic linear FE analysis results for W7. Displacement and stress (*y*-direction) contour plots at the moment of maximum displacements and stresses. The pressure distributions along the height of the crownwalls at the moment of maximum total wave force are plotted as dashed lines while at the moment of maximum displacements and stresses are plotted as solid lines. The points of application of the total wave force (F) at the moment of maximum displacements and stresses are indicated (blue arrows) as well as the location of the maximum tensile stresses (black dots).

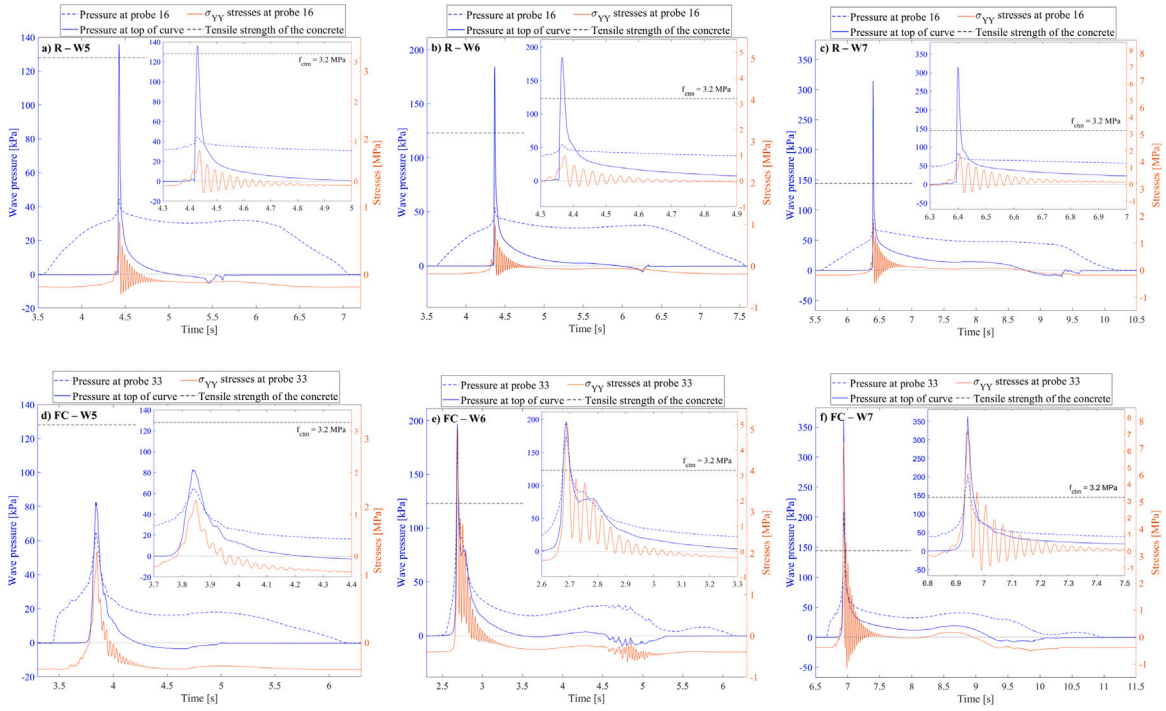

Fig. 16. Stresses in the *y*-direction at the location of maximum tensile stresses are plotted in orange on the right *y*-axis. The wave pressure at the location of maximum tensile stress (dashed line) and wave pressure at the top of the curves of the crownwalls (solid line) are plotted in blue on the left *y*-axis. The tensile strength of the concrete, $f_{ctm} = 3.2$ MPa, is represented with a black dashed line.

coupled numerical approach. Hydrodynamic pressures were obtained through CFD simulations in OpenFOAM and applied as input to structural analyses performed in DIANA FEA.

Despite having the same cross-sectional area, the FC crownwall, due to its different shape, experiences significantly higher wave-induced forces and tensile stresses than the R crownwall. This difference arises from its continuous curvature and narrower critical cross-section, which amplify stress localization and necessitate additional reinforcement for structural integrity.

From a hydraulic perspective, the FC crownwall shows a tendency toward improved performance in reducing overtopping volumes under intermediate wave conditions (i.e., when the relative freeboard is slightly greater than one). At lower relative freeboard values, overtopping becomes primarily driven by wave crests passing directly over the crownwall, limiting the differences between the two configurations.

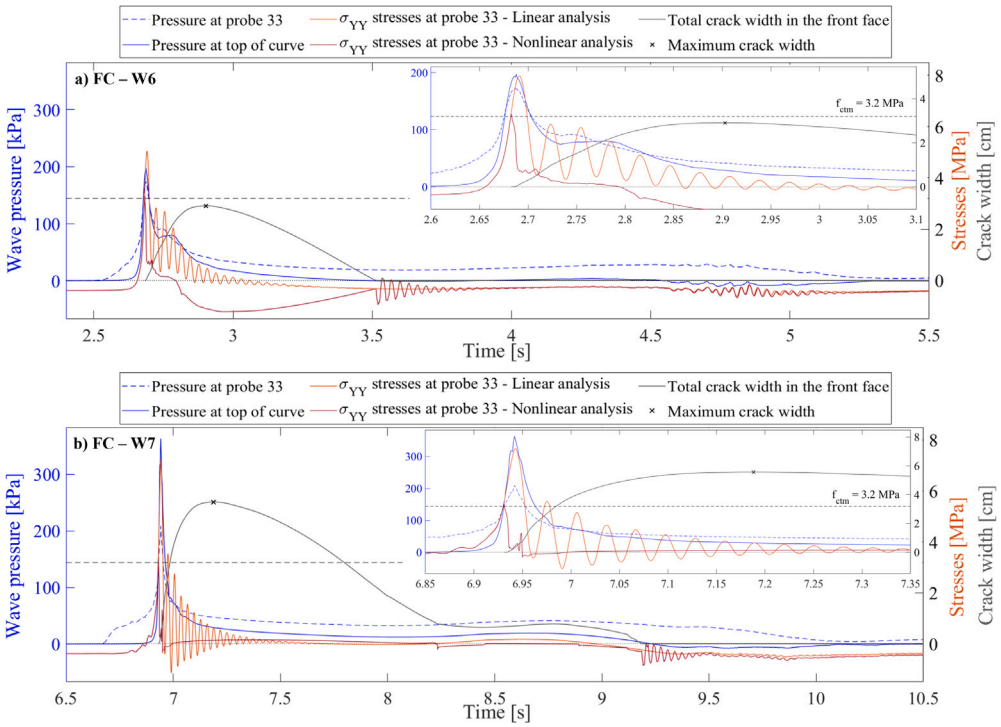

Fig. 17. Results of nonlinear analysis of the FC crownwall under wave load by (a) W6 and (b) W7. Left axis in blue: wave pressure–time series at probe 33 and at the top of the curve. Right axis: time series of the resulting stresses in the *y*-direction at probe 33 of the linear and nonlinear FE analysis, in orange, and total crack width in the front face of the crownwall.

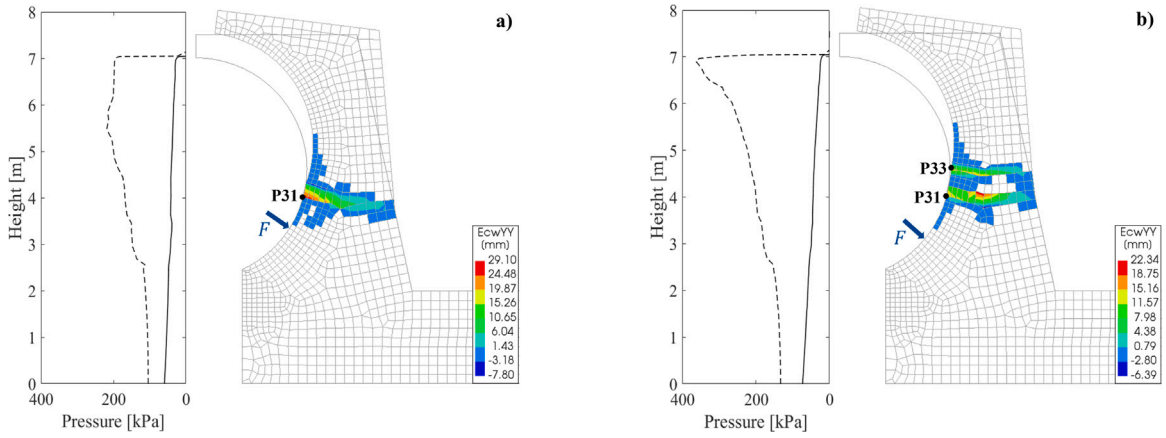

Fig. 18. Contour plots of the crack widths in the FC crownwall under wave load from (a) W6 and (b) W7 wave conditions. Pressure distribution along the height of the crownwall at the moment of maximum cracking is shown as solid lines, and the pressure distribution at the moment of maximum total wave force is shown as dashed lines.

At higher relative freeboard values, both crownwall shapes similarly redirect the incident waves offshore, and the hydraulic advantage of the FC crownwall becomes less pronounced. While some indication of improved hydraulic efficiency exists for the FC design under specific conditions, this comes at the cost of increased structural demand. It experiences wave forces up to 2.5 times greater than those acting on the R crownwall, along with longer pressure impulse durations. These factors increase the stress levels and dynamic amplification in the FC crownwall, raising the likelihood of cracking under severe loading. In contrast, the R crownwall shows a more linear stress distribution and lower overall forces, although it can experience localized peak pressures due to the Confined-Crest Impact phenomenon.

The findings underscore the importance of integrating dynamic structural analysis into the crownwall design process. Although the FC crownwall provides superior overtopping reduction, the R crownwall remains the most practical and cost-effective solution for vertical breakwaters subjected to impulsive wave loads. Future research should focus on optimizing crownwall geometries to achieve a better balance between hydraulic efficiency and structural resilience.

CRediT authorship contribution statement

Lára M. Gísladóttir: Conceptualization, Data curation, Formal analysis, Investigation, Methodology, Software, Visualization, Writing – original draft, Writing – review & editing. **Myrta Castellino:** Conceptualization, Data curation, Formal analysis, Investigation, Methodology, Software, Visualization, Writing – original draft, Writing – review & editing. **Dimitrios Dermentzoglou:** Software, Writing – review & editing. **Max A.N. Hendriks:** Software, Writing – review & editing. **Paolo de Girolamo:** Writing – review & editing. **Marcel R.A. van Gent:** Writing – review & editing. **Alessandro Antonini:** Conceptualization, Investigation, Methodology, Supervision, Writing – review & editing.

Declaration of Generative AI and AI-assisted technologies in the writing process

During the preparation of this work the authors used *ChatGPT* in order to improve readability and language of the text. After using this technology, the authors reviewed and edited the content as needed and take full responsibility for the content of the published article.

Declaration of competing interest

The authors declare the following financial interests/personal relationships which may be considered as potential competing interests: Co-author Marcel R.A. van Gent is Editor-in-Chief of Coastal Engineering. The manuscript has been handled by one of the associate editors, who selected the reviewers and evaluated the manuscript without any influence on these decisions by the Editor-in-Chief. If there are other authors, they declare that they have no known competing financial interests or personal relationships that could have appeared to influence the work reported in this paper.

Data availability

Data will be made available on request.

References

Antonini, A., Dermentzoglou, D., Almeida, d.E., Hofland, B., Celli, D., Pasquali, D., Risio, d.M., Castellino, M., de Girolamo, P., 2023. Physical experiments on overhanging parapets under non-breaking wave conditions. Coast. Eng. Proc. 37, http://dx.doi.org/10.9753/icce.v37.structures.81, URL: https://icce-ojs-tamu.tdl.org/icce/article/view/12937.structures.81.

Antonini, A., William Brownjohn, J.M., Dassanayake, D., Raby, A., Bassit, J., Pappas, A., D'Ayala, D., 2021. A Bayesian inverse dynamic approach for impulsive wave loading reconstruction: Theory, laboratory and field application. Coast. Eng. 168, 103920. http://dx.doi.org/10.1016/j.coastaleng.2021.103920, URL: https://www.sciencedirect.com/science/article/pii/S0378383921000806.

Attili, T., Heller, V., Triantafyllou, S., 2023a. Scaling approaches and scale effects in wave–flexible structure interaction. J. Fluids Struct. 123, 103987. http://dx.doi.org/10.1016/j.jfluidstructs.2023.103987.

Attili, T., Heller, V., Triantafyllou, S., 2023b. Wave impact on rigid and flexible plates. Coast. Eng. 182, 104302.

Bagnold, R., 1939. Interim report on wave-pressure research.(includes plates and photographs). J. Inst. Civ. Eng. 12 (7), 202–226.

Castellino, M., 2024. Confined-crest impact: The influence of the Toe Berm on the impulsive forces. J. Waterw. Port Coast. Ocean. Eng. 150 (5), 04024008.

Castellino, M., Lara, J.L., Romano, A., Losada, I.J., De Girolamo, P., 2018a. Wave loading for recurved parapet walls in non-breaking wave conditions: analysis of the induced impulsive forces. Coast. Eng. Proc. 36, 34.

Castellino, M., Romano, A., Lara, J.L., Losada, I.J., De Girolamo, P., 2021. Confined-crest impact: Forces dimensional analysis and extension of the Goda's formulae to recurved parapets. Coast. Eng. 163, 103814.

Castellino, M., Sammarco, P., Romano, A., Martinelli, L., Ruol, P., Franco, L., De Girolamo, P., 2018b. Large impulsive forces on recurved parapets under non-breaking waves. a numerical study. Coast. Eng. 136, 1–15.

Chen, X., Hofland, B., Molenaar, W., Capel, A., Van Gent, M.R., 2019. Use of impulses to determine the reaction force of a hydraulic structure with an overhang due to wave impact. Coast. Eng. 147, 75–88.

Cooker, M.J., Peregrine, D., 1995. Pressure-impulse theory for liquid impact problems. J. Fluid Mech. 297, 193–214.

Cuomo, G., Allsop, W., Bruce, T., Pearson, J., 2010. Breaking wave loads at vertical seawalls and breakwaters. Coast. Eng. 57 (4), 424–439.

Cuomo, G., Lupoi, G., Shimosako, K.-I., Takahashi, S., 2011. Dynamic response and sliding distance of composite breakwaters under breaking and non-breaking wave attack. Coast. Eng. 58 (10), 953–969.

De Almeida, E., Hofland, B., 2020. Validation of pressure-impulse theory for standing wave impact loading on vertical hydraulic structures with short overhangs. Coast. Eng. 159, 103702.

De Almeida, E., Hofland, B., 2021. Standing wave impacts on vertical hydraulic structures with overhangs for varying wave fields and configurations. J. Coast. Hydraul. Struct. 1.

De Girolamo, P., Castellino, M., Romano, A., 2019. Improvement in workability of terminals placed along the inner side of port vertical breakwaters by means of recurved parapet walls. WIT Trans. Built Environ. 187, 23–30.

Dermentzoglou, D., Castellino, M., De Girolamo, P., Partovi, M., Schreppers, G.J., Antonini, A., 2020. Crownwall failure analysis through finite element method. J. Mar. Sci. Eng. 9 (1), 35.

DIANA FEA BV, 2021. DIANA finite element analysis - user's manual 10.5.

E.N. 1992-1-1, 2004. Eurocode 2: Design of Concrete Structures - Part 1-1: General Rules and Rules for Buildings. (EN 1992-1-1), European Committee for Standardization (CEN), Brussels, Belgium, URL: https://www.phd.eng.br/wp-content/uploads/2015/12/en.1992.1.1.2004.pdf.

EurOtop, M., 2018. In: van der Meer, J., Allsop, N., Bruce, T., De Rouck J, J., Kortenhaus, A., Pullen, T., Schüttrumpf, H., Troch, P., Zanuttigh, B. (Eds.), Manual on Wave Overtopping of Sea Defences and Related Structures. www.overtopping-manual.com.

Goda, Y., 1994. Dynamic response of upright breakwaters to impulsive breaking wave forces. Coast. Eng. 22 (1–2), 135–158.

Goeijenbier, B., Bricker, J., Antonini, A., Malara, G., Hendriks, M., van der Ham, H., 2021. Structural optimisation and behaviour of the breakwater integrated oscillating water column device: A combined 3D CFD and structural FEM analysis. J. Coast. Hydraul. Struct. 1, http://dx.doi.org/10.48438/JCHS.2021.0002.

Higuera, P., Lara, J.L., Losada, I.J., 2013a. Realistic wave generation and active wave absorption for Navier–Stokes models: Application to openfoam®. Coast. Eng. 71, 102–118.

Higuera, P., Lara, J.L., Losada, I.J., 2013b. Simulating coastal engineering processes with openfoam®. Coast. Eng. 71, 119–134.

Higuera, P., Lara, J.L., Losada, I.J., 2014. Three-dimensional interaction of waves and porous coastal structures using openfoam®. Part I: Formulation and validation. Coast. Eng. 83, 243–258.

Hirt, C., Nichols, B., 1981. Volume of fluid (VOF) method for the dynamics of free boundaries. J. Comput. Phys. 39 (1), 201–225. http://dx.doi.org/10.1016/0021-9991(81)90145-5.

Huang, J., Chen, G., Lowe, R.J., 2022. Experimental study on the probability of different wave impact types on a vertical wall with horizontal slab by separation of quasi-static wave impacts. J. Mar. Sci. Eng. 10 (5), 615.

Humar, J., 2012. Dynamics of Structures. CRC Press.

Kisacik, D., Troch, P., Van Bogaert, P., 2012. Description of loading conditions due to violent wave impacts on a vertical structure with an overhanging horizontal cantilever slab. Coast. Eng. 60, 201–226.

Kisacik, D., Troch, P., Van Bogaert, P., Caspeele, R., 2014. Investigation of uplift impact forces on a vertical wall with an overhanging horizontal cantilever slab. Coast. Eng. 90, 12–22.

Kortenhaus, A., Oumeraci, H., 1998. Classification of wave loading on monolithic coastal structures. In: Coastal Engineering 1998. pp. 867–880.

Kortenhaus, A., Pearson, J., Bruce, T., Allsop, N., Van der Meer, J., 2004. Influence of parapets and recurves on wave overtopping and wave loading of complex vertical walls. In: Coastal Structures 2003. pp. 369–381.

Larsen, B.E., Fuhrman, D.R., Roenby, J., 2019. Performance of interfoam on the simulation of progressive waves. Coast. Eng. J. 61 (3), 380–400.

Martinelli, L., Ruol, P., Volpato, M., Favaretto, C., Castellino, M., De Girolamo, P., Franco, L., Romano, A., Sammarco, P., 2018. Experimental investigation on non-breaking wave forces and overtopping at the recurved parapets of vertical breakwaters. Coast. Eng. 141, 52–67.

Naeimi, N., Moustafa, M.A., 2017. Three-dimensional finite element modeling of UHPC using total strain crack models. In: AFGC-ACI-Fib-RILEM Int. Symp. Ultra-High Perform. Fibre-Reinforced Concr. UHPFRC. pp. 313–324.

Negro, V., Martín-Antón, M., del Campo, J.M., López-Gutiérrez, J.S., Esteban, M.D., 2018. Crown walls in mass and reinforced concrete: The way to aesthetics in maritime works. In: Coasts, Marine Structures and Breakwaters 2017: Realising the Potential. ICE Publishing, pp. 471–480.

Oumeraci, H., Kortenhaus, A., 1994. Analysis of the dynamic response of caisson breakwaters. Coast. Eng. 22 (1–2), 159–183.

Oumeraci, H., Partenscky, H., Tautenhain, E., Flume, L.W., Nickels, H., 1992. 13. Large-scale model investigation: a contribution to the revival of vertical breakwaters. In: Coastal Structures and Breakwaters: Proceedings of the Conference Organized By the Institution of Civil Engineers, and Held in London on 6-8 November 1991. Thomas Telford, p. 207.

Pearson, J., Bruce, T., Allsop, W., Kortenhaus, A., van der Meer, J., 2005. Effectiveness of recurve walls in reducing wave overtopping on seawalls and breakwaters. In: Coastal Engineering 2004: (in 4 Volumes). World Scientific, pp. 4404–4416.

Pedersen, J., Burcharth, H.F., 1992. Wave forces on crown walls. In: Coastal Engineering 1992. pp. 1489–1502.

Ramkema, C., 1978. A model law for wave impacts on coastal structures. In: Coastal Engineering 1978. pp. 2308–2327.

Ravindar, R., Sriram, V., Schimmels, S., Stagonas, D., 2019. Characterization of breaking wave impact on vertical wall with recurve. ISH J. Hydraul. Eng. 25 (2), 153–161. http://dx.doi.org/10.1080/09715010.2017.1391132.

Rots, J.G., 1991. Smeared and discrete representations of localized fracture. Curr. Trends Concr. Fract. Res. 45–59.

Schoonees, T., 2014. Impermeable Recurve Seawalls to Reduce Wave Overtopping (Masters thesis). Stellenbosch: Stellenbosch University.

Selby, R.G., 1994. Three-dimensional constitutive relations for reinforced concrete/by Robert Gordon Selby. Bibliothèque nationale du Canada,Ottawa, National Library of Canada.

Shimosako, K., Takahashi, S., Tanimoto, K., 1995. Estimating the sliding distance of composite breakwaters due to wave forces inclusive of impulsive forces. In: Coastal Engineering 1994. pp. 1580–1594.

Słowik, M., 2019. The analysis of failure in concrete and reinforced concrete beams with different reinforcement ratio. Arch. Appl. Mech. 89, 885–895.

Stagonas, D., Lara, J.L., Losada, I.J., Higuera, P., Jaime, F.F., Muller, G., 2014. Large scale measurements of wave loads and mapping of impact pressure distribution at the underside of wave recurves. In: Proceedings of the HYDRALAB IV Joint User Meeting. pp. 1–10.

Stagonas, D., Ravindar, R., Sriram, V., Schimmels, S., 2020. Experimental evidence of the influence of recurves on wave loads at vertical seawalls. Water 12 (3), 889.

Streicher, M., Kortenhaus, A., Marinov, K., Hirt, M., Hughes, S., Hofland, B., Scheres, B., Schüttrumpf, H., 2019. Classification of bore patterns induced by storm waves overtopping a dike crest and their impact types on dike mounted vertical walls–a large-scale model study. Coast. Eng. J. 61 (3), 321–339.

Takahashi, S., 2002. Design of vertical breakwaters. PHRI reference document nr. 34.

Takahashi, S., Tsuda, M., Suzuki, K., Shimosako, K.i., 1999. Experimental and fem simulation of the dynamic response of a caisson wall against breaking wave impulsive pressures. In: Coastal Engineering 1998. pp. 1986–1999.

Valdecantos, V.N., Gutiérrez, J.S.L., Flors, J.I.P., Molines, J., 2014. Discussion: Comparative study of breakwater crown wall–calculation methods. In: Proceedings of the Institution of Civil Engineers-Maritime Engineering, vol. 167, Thomas Telford Ltd, pp. 154–155.

Vecchio, F.J., Collins, M.P., 1986. The modified compression-field theory for reinforced concrete elements subjected to shear. ACI J. 83 (2), 219–231.

Wood, D., Peregrine, D., 1996. Wave impact beneath a horizontal surface. In: Coastal Engineering 1996. pp. 2573–2583.